Article

Self-Organizing Core–Shell Nanostructures: Spontaneous Accumulation of Dye in the Core of Doped Silica Nanoparticles

Enrico Rampazzo, Sara Bonacchi, Marco Montalti, Luca Prodi, and Nelsi Zaccheroni

J. Am. Chem. Soc., **2007**, 129 (46), 14251-14256• DOI: 10.1021/ja073150j • Publication Date (Web): 25 October 2007

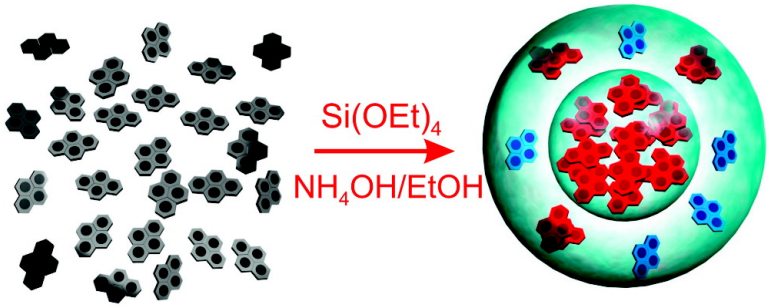

J|A|C|S
ARTICLES
Published on Web 10/25/2007

Self-Organizing Core−Shell Nanostructures: Spontaneous Accumulation of Dye in the Core of Doped Silica Nanoparticles

Enrico Rampazzo, Sara Bonacchi, Marco Montalti,* Luca Prodi, and Nelsi Zaccheroni

Contribution from the Dipartimento di Chimica "G. Ciamician", Latemar Unit, Università di Bologna, Via Selmi 2, I-40126 Bologna, Italy

Received May 4, 2007; E-mail: marco.montalti2@unibo.it

Abstract: The process of formation of silica nanoparticles doped with a newly synthesized pyrene derivative has been investigated by means of fluorescence steady-state and time-resolved spectroscopy. The changes in the photophysical properties of the fluorophore were correlated to the increase of the nanoparticles hydrodynamic volume measured via dynamic light scattering (DLS) allowing us to determine the radial profile of the concentration of the dye. Experiments performed at a "low" degree of doping show that the fluorophore is almost completely included considerably before the end of the nanoparticles growth, allowing us to identify a self-organizing core−shell substructure. A strong enhancement of the fluorescence of the dye and a corresponding increase of its excited-state lifetime was observed upon its inclusion as a result of the shielding effect from molecular oxygen due to the silica matrix, a situation confirmed by the absence of the oxygen singlet emission in the near-infrared luminescence spectra. In the case of "high" loading, on the other hand, a heavily doped core showing an excimeric-like emission is first formed. Further growth leads to the formation of layers where the concentration of dye gradually decreases and the monomeric emission becomes relevant. The effect of the degree of doping on the kinetics of growth is also reported. At both concentration regimes, ultrafiltration experiments revealed the complete inclusion of the dye molecules. The average number of dye molecule per nanoparticles was also determined.

Introduction

Fluorescent silica nanoparticles present considerable advantages with respect to conventional molecular dyes in the design of fluorescent labeling agents and chemosensors, especially by virtue of their intense fluorescence and photostability.[1−6] The large number of dye units housed in the relatively small volume of a single nanoparticle in fact supply, in the same excitation conditions, a fluorescence signal which is in some cases 10^4 to 10^5 times stronger with respect to a single dye molecule in aqueous solution.[2a] As a consequence, the brightness of these materials, defined as the product of the fluorescence quantum yield (Φ) of a dye and their molar decadic absorption coefficient ϵ,[2a,7] is in some cases even higher with respect to semiconductor nanocrystals (quantum dots) both upon one-photon[2a] and two-photon[4a] excitation. Besides the trivial additive effect on the excitation efficiency due to the copresence of many absorbers in each nanoparticle (hence to a large ϵ value), other more sophisticated aspects must be taken into account in order to generalize the photophysical and photochemical behavior of doped silica nanoparticles. Dye molecules in fact experience inside the silica matrix an environment which is significantly less polar than water, and their mobility is strongly reduced.[5a] Such change in polarity is known to have strong effects on the photophysical properties of the molecules influencing the

(1) (a) Verhaegh, N. A. M.; van Blaaderen, A. *Langmuir* **1994**, *10*, 1427−1438. (b) van Blaaderen, A.; Imhof, A.; Hage, W.; Vrij, A. *Langmuir* **1992**, *8*, 1514−1517. (c) Stöber, W.; Fink, A.; Bohn, E. *J. Colloid Interface Sci.* **1968**, *26*, 62.
(2) (a) Wang, L.; Wang, K. M.; Santra, S.; Zhao, X. J.; Hilliard, L. R.; Smith, J. E.; Wu, J. R.; Tan, W. H. *Anal. Chem.* **2006**, *78*, 646−654. (b) Smith, J. E.; Wang, L.; Tan, W. T. *TrAC, Trends Anal. Chem.* **2006**, *25*, 848−855. (c) Wang, L.; Tan, W. H. *Nano Lett.* **2006**, *6*, 84−88. (d) Yao, G.; Wang, L.; Wu, Y. R.; Smith, J.; Xu, J. S.; Zhao, W. J.; Lee, E. J.; Tan, W. H. *Anal. Bioanal. Chem.* **2006**, *385*, 518−524. (e) Wang, L.; Yang, C. Y.; Tan, W. H. *Nano Lett.* **2005**, *5*, 37−43. (f) Zhao, X. J.; Bagwe, R. P.; Tan, W. H. *Adv. Mater.* **2004**, *16*, 173. (g) Lian, W.; Litherland, S. A.; Badrane, H.; Tan, W. H.; Wu, D. H.; Baker, H. V.; Gulig, P. A.; Lim, D. V.; Jin, S. G. *Anal. Biochem.* **2004**, *334*, 135−144. (h) Qhobosheane, M.; Santra, S.; Zhang, P.; Tan, W. H. *Analyst* **2001**, *126*, 1274−1278.
(3) (a) Nagl, S.; Schaeferling, M.; Wolfbeis, O. S. *Microchim. Acta* **2005**, *151*, 1−21. (b) Kim, S.; Pudavar, H. E.; Prasad, P. N. *Chem. Commun.* **2006**, 2071−2073. (c) Buck, S. M.; Koo, Y. E. L.; Park, E.; Xu, H.; Philbert, M. A.; Brasuel, M. A.; Kopelman, R. *Curr. Opin. Chem. Biol.* **2004**, *8*, 540−546. (d) Rossi, L. M.; Shi, L. F.; Quina, F. H.; Rosenzweig, Z. *Langmuir* **2005**, *21*, 4277−4280. (e) Rossi, L. M.; Shi, L. F.; Rosenzweig, N.; Rosenzweig, Z. *Biosens. Bioelectron.* **2006**, *21*, 1900−1906.
(4) (a) Ow, H.; Larson, D. R.; Srivastava, M.; Baird, B. A.; Webb, W. W.; Wiesner, U. *Nano Lett.* **2005**, *5*, 113−117. (b) Burns, A.; Ow, H.; Wiesner, U. *Chem. Soc. Rev.* **2006**, *35*, 1028−1042.
(5) (a) Montalti, M.; Prodi, L.; Zaccheroni, N.; Battistini, N.; Marcuz, S.; Mancin, F.; Rampazzo, E.; Tonellato, U. *Langmuir* **2006**, *22*, 5877−5881. (b) Montalti, M.; Prodi, L.; Zaccheroni, N. *J. Mater. Chem.* **2005**, *15*, 2810−2814. (c) Montalti, M.; Prodi, L.; Zacheroni, N.; Zattoni, A.; Reschiglian, P.; Falini, G. *Langmuir* **2004**, *20*, 2989−2991. (d) Montalti, M.; Prodi, L.; Zaccheroni, N.; Falini, G. *J. Am. Chem. Soc.* **2002**, *124*, 13540−13546.
(6) (a) Teolato, P.; Rampazzo, E.; Arduini, M.; Mancin, F.; Tecilla, P.; Tonellato, U. *Chem. Eur. J.* **2007**, *8*, 2238−2245. (b) Mancin, F.; Rampazzo, E.; Tecilla, P.; Tonellato, U. *Chem. Eur. J.* **2006**, *12*, 1844−1854. (c) Rampazzo, E.; Brasola, E.; Marcuz, S.; Mancin, F.; Tecilla, P.; Tonellato, U. *J. Mater. Chem.* **2005**, *15*, 2687−2696. (d) Brasola, E.; Mancin, F.; Rampazzo, E.; Tecilla, P.; Tonellato, U. *Chem. Commun.* **2003**, 3026−3027.
(7) Braslavsky, S. E. *Pure Appl. Chem.* **2007**, *79*, 293−465.

energies of the electronic states and the rate constants of the electronic transitions while the limited mobility may slow down vibrational relaxation and reorganization processes preventing nonradiative deactivation from occurring. The silica matrix, on the other hand, does also play a shielding role sequestrating the fluorophore from the environment and protecting it from diffusional quenching due to other species like molecular oxygen. In order to optimize such a segregation effect some authors have proposed multistep synthesis of core−shell structures in order to confine the dye in an inner region protected by an undoped silica layer.[4a] In this paper we demonstrate that similar structures spontaneously form when pyrene-doped silica nanoparticles are prepared via the Stöber−Van Blaaderen method using the pyrene derivative **1**.[1] This dye is an excellent probe for exploring the inner structure of the nanoparticles.[8] The photophysical properties of pyrene are, in fact, affected by the local environment and concentration, and for these reasons it has been extensively used for characterizing nanostructures such as micellar systems.[8f,g] In particular, we observed that its fluorescence quantum yield increases an order of magnitude when it is sequestered inside silica nanoparticles as an effect of its segregation from atmospheric oxygen. Such a huge difference in the fluorescence properties allows us to distinguish the included molecules from free ones during the nanoparticles growth and, therefore, to follow the process in real time. Moreover, as we reported for other systems,[8a] in the case of pyrene interaction of excited molecules with ground-state ones does not cause self-quenching,[5c] but excimer formation. As a consequence, the ratio between the intensities of the monomeric and excimeric fluorescence bands gives precious information about the average distances between the pyrene moieties and hence an indirect measure of the local concentration of the dye.[8f,g] By combining these two effects the inclusion of the dye can be followed during the layer after layer growth of the nanoparticles. The correlation of the photophysical measurements to the hydrodynamic volume measured by dynamic light scattering (DLS)[9] allows us to locate the fraction of dye molecules incorporated in each layer during the different stages of the growth. We would like to stress that, since the grafting of the dye is covalent, no reorganization of the structure, as observed in the case of micelles, is expected to take place; as a consequence, the degree of dye accumulation observed in each layer during the growth will be maintained in the final structure. The scenario revealed is surprising, and it discloses a new feature of doped silica nanoparticles: the concentration dishomogeneity[2c,e,5] of the dye and its preponderant accumulation in a restricted core. The conventional picture of organically doped nanoparticles as a scaffold in which the active molecules are homogenously dispersed is hence too simplified and unrealistic: the intrinsic core−shell structure of this material has to be considered in the design of new more sophisticated and efficient systems.

(8) (a) Montalti, M.; Prodi, L.; Zaccheroni, N.; Battistini, G. *Langmuir* **2004**, *20*, 7884−7886. (b) Montalti, M.; Prodi, L.; Zaccheroni, N.; Baxter, R.; Teobaldi, G.; Zerbetto, F. *Langmuir* **2003**, *19*, 5172−5174. (c) Montalti, M.; Zaccheroni, N.; Prodi, L.; O'Reilly, N.; James, S. L. *J. Am. Chem. Soc.* **2007**, *129*, 2418−2419. (d) Karpovich, D. S.; Blanchard, G. J. *J. Phys. Chem.* **1995**, *99*, 3951−3958. (e) Kalyanasundaram, K.; Thomas, J. K. *J. Am. Chem. Soc.* **1977**, *99*, 2039−2044. (f) Turro, N. J.; Kuo, P.-L. *Langmuir* **1987**, *3*, 773−777. (g) Rharbi, Y.; Li, M.; Winnik, M. A.; Hahn, K. G., Jr. *J. Am. Chem. Soc.* **2000**, *122*, 6242−6251. (h) Yihwa, C.; Kellermann, M.; Becherer, M.; Hirsch, A.; Bohne, C. *Photochem. Photobiol. Sci.* **2007**, *6*, 525−531.

Experimental Section

General. All solvents and reagents were purchased from Sigma-Aldrich and used without further purification. Thin-layer chromatography (TLC) was performed using Fluka silica 60 precoated aluminum cards (0.25 mm) with 254 nm fluorescent indicator.

NMR Experiments. NMR spectra were recorded with a Varian Inova 300 MHz spectrometer. Chemical shifts are reported relative to tetramethylsilane as internal standard.

Mass Spectrometry. Electrospray ionization mass spectrometry (ESI-MS) measurements were made by means of a Navigator LC/MS Thermo Quest Finningan mass spectrometer and with an Agilent Technologies LC/MSD Trap SL mass spectrometer. For the latter a flow injection analysis method was used.

Ultrafiltration Experiments. Ultrafiltration and filtration of nanoparticles were carried out in a 75 mL stainless steel−glass solvent-resistant stirred cell purchased from Millipore (47 mm filters). The ultrafiltration experimental setup included Amicon regenerated cellulose membranes (100 kDa cutoff) and an auxiliary reservoir (800 mL) filled with ethanol and equipped with a concentration selector valve. For simple filtration purposes the same filtration cell has been employed without the reservoir using Durapore membrane filters (PVDF 0.45, 0.22, 0.10 μm) drained by means of a Whatman GF/A glass microfiber filter. Quantification of the dye not included in the nanoparticles was carried out by measuring the absorbance at 345 nm and the volumes of collected ultrafiltrate solutions for each sample.

Particles Size Distribution. Dynamic light scattering was used for the determination of the silica nanoparticles size distributions employing a Malvern Nano ZS instrument with a 633 nm laser diode. Formation kinetics were carried at 30 °C in a quartz cuvette of 1 cm optical path length. Reaction mixtures subjected to these measurements were extensively filtered through 0.1 μm Durapore membrane filters before addition of tetraethoxysilane (TEOS). Kinetics profile were obtained monitoring both hydrodynamic diameter and derived count rate. The latter parameter is the calculated mean count rate that will obtained if no attenuation is used. During the kinetic progress the attenuation values were set to keep the mean count rate less than 1000 kcps (kilo counts per second).

The concentrations of nanoparticles were estimated using the Concentration Protein Utilities tool of the Malvern Dispersion Technology Software 5.00, using the scattering intensities of toluene as standard. Before each determination nanoparticles solutions were filtered through 0.22 μm Durapore filters. The scattering intensity of each sample was obtained making the difference with the one of the dispersant (ethanol) in the same conditions. Control experiments were carried out by performing measurements with an aqueous solution of β-cyclodextrin filtered by means of a Whatman Anotop 0.020 μm filter.

Photophysical Measurements. UV−vis absorption spectra were performed at 25 °C by means of a Perkin-Elmer Lambda 45 spectrophotometer. Quartz cuvettes with optical path length of 1 cm were used. The fluorescence spectra were recorded with an Edinburgh FLS920 equipped with a Hamamatsu R928P photomultiplier for the UV−vis region while a germanium detector was used for the near-infrared (NIR) spectra. The same instrument connected to a PCS900 PC card was used for the time-correlated single-photon counting (TCSPC) experiments. When necessary, deoxygenated samples were prepared by flowing N_2 in the solutions in a customized airtight quartz cuvette equipped with a screwable closure cap.

Synthesis of Compound 1. Triethoxy(3-isocyanatopropyl)silane (3.30 mL, 13.3 mmol) and triethylamine (0.20 mL, 1.43 mmol) were added to a solution of 1-methylaminopyrene hydrochloride (0.236 g, 0.88 mmol) in anhydrous dimethylformamide (4.0 mL). The mixture was stirred at room temperature for 5 h monitoring the reaction by TLC (petroleum ether/ethylacetate 1:4, $R_f = 0.64$). A minimum amount

(9) Jillavenkatesa, A.; Dapkunas, S. J.; Lum, L. S. H. *NIST Spec. Publ.* **2001**, 960-1, 95−124.

of dichloromethane was added to solubilize the heterogeneous reaction mixture, and precipitation was induced by addition of 100 mL of petroleum ether. The white solid, containing compound **1**, was recovered by filtration, and after washing with petroleum ether, it was dissolved in tetrahydrofuran and filtered. The resulting solution, containing **1**, was concentrated by rotary evaporation; 100 mL of petroleum ether was then slowly added. Compound **1** (319 mg, 76% yield) was finally recovered as a slightly yellow solid by centrifugation and dried under vacuum.

^{1}H NMR (300 MHz, $CDCl_3$, 25 °C) δ (ppm): 0.58 (t, J = 8.1 Hz, 2H, $NCH_2CH_2CH_2$–Si), 1.14 (t, J = 7.0 Hz, 9H, $NCH_2CH_2CH_2-Si-(OCH_2CH_3)_3$), 1.58 (m, 2H, $NHCH_2CH_2CH_2$–Si), 3.15 (q, 2H, J = 6.5 Hz, $NHCH_2CH_2CH_2$–Si), 3.72 (q, J = 7.0 Hz, 6H, $NHCH_2CH_2CH_2-Si-(OCH_2CH_3)_3$), 4.71 (t, J = 5.3 Hz, 1H, $CONHCH_2CH_2CH_2$–Si), 4.88 (t, J = 5.0 Hz, 1H, $CONHCH_2$Pyrene), 4.96 (d, J = 5.0 Hz, 2H, $NHCH_2$Pyrene), 7.88 (d, J = 7.9 Hz, 1H), 7.97 (m, 3H), 8.03 (d, J = 2.8 Hz, 1H), 8.06 (d, J = 4.3 Hz, 1H), 8.12 (d, J = 7.8 Hz, 2H), 8.21 (d, J = 9.2 Hz, 1H) $NHCH_2$*Pyrene*.

^{13}C NMR (75.5 MHz, $CDCl_3$, 25 °C) δ (ppm): 7.51 ($NCH_2CH_2CH_2$–Si), 18.2 ($NCH_2CH_2CH_2-Si-(OCH_2CH_3)_3$), 23.6 ($NCH_2CH_2CH_2$–Si), 42.8 ($NHCH_2$Pyrene), 43.0 ($NHCH_2CH_2CH_2$–Si), 58.4 ($NHCH_2CH_2CH_2-Si-(OCH_2CH_3)_3$), 122.9, 124.7, 124.9, 125.1, 125.2, 125.5, 125.9, 126.7, 127.3, 127.9, 128.8, 130.7, 131.2, 132.1 ($NHCH_2$*Pyrene*), 157.9 ($NHCONHCH_2$Pyrene). ESI-MS, *m/z*: 479 [M + H]$^+$.

Nanoparticles Synthesis. Samples of silica nanoparticles doped with two different concentrations of pyrene derivative **1** were investigated. The amounts of fluorescent silane introduced were 0.1% and 1.0% mol/mol versus TEOS for samples **N1A** and **N1B**, respectively; the actual concentration of the dye was checked by UV–vis absorption spectroscopy. Nanoparticles synthesis was carried out in 30 mL tubes equipped with screw cap at 30 °C. In a typical procedure, 650 μL of aqueous ammonia (28–30 wt % NH_3 in water) was added to 13.0 mL of absolute ethanol. To this solution was added the desiderated amount of ethanolic solution of pyrene derivative **1** (7.04 mM, 50 and 500 μL for the 0.1% and 1.0% samples, respectively). This solution was stirred (600 rpm) for 30 min in order to hydrolyze the ethoxysilane group. The absence of the excimeric band in the fluorescence spectrum recorded upon excitation at 345 nm after this step indicated that condensation of the dye does not take place in these conditions. The formation of nanoparticles and the photophysical and DLS measurements started after the addition of 78.5 μL of TEOS. The reaction mixture was stirred during the nanoparticles formation. Small samples (100 μL) taken at different reaction times were diluted in 3.0 mL of ethanol in order to slow down the reaction, and photophysical characterization was performed. The obtained colloidal suspension was then filtered through Durapore membrane filters (0.22 μm) and purified by ultrafiltration process.

Kinetic Models. Silica nanoparticles formation results from a nucleation–growth process which involves hydrolysis (eq 1) of the TEOS precursor in ethanol followed by condensation[1c,10] (eq 2):

$$Si(OEt)_4 + 4H_2O \xrightarrow{EtOH,\ NH_3} Si(OH)_4 + 4EtOH \quad (1)$$

$$Si(OH)_4 \xrightarrow{EtOH,\ NH_3} SiO_2 + H_2O \quad (2)$$

The overall rate of the particle growth is limited by the first-order hydrolysis rate of the alkoxide,[10] and, taking into account the induction time t_n due to the nucleation, the volume $V(t)$ of the nanoparticles increases during the time according to equation:

$$V(t) = V_f\{1 - \exp[-k(t - t_n)]\} \quad (3)$$

(10) van Blaaderen, A.; van Geest, J.; Vrij, A. *J. Colloid Interface Sci.* **1992**, *154*, 481–501.

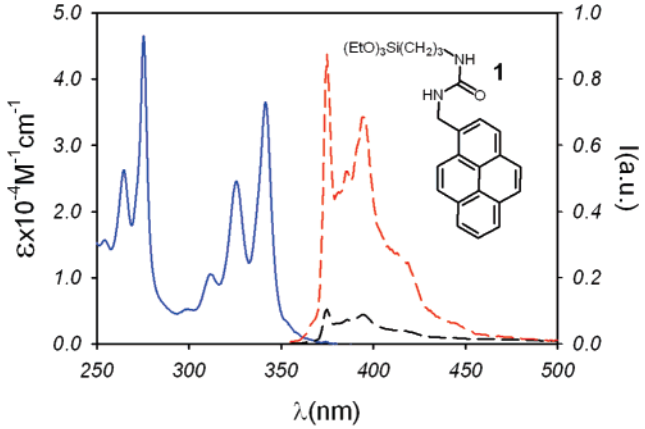

Figure 1. Absorption spectrum of compound **1** (blue line) in ethanol solution. Fluorescence spectra of compound **1** in aerated (black dashed line) and deoxygenated (red dashed line) ethanol solution (λ_{exc} = 345 nm).

where V_f is the final volume reached by the nanoparticles and k is the kinetic constant of the rate-determining step, namely, reaction 1. In this model it is assumed that the number of growing particles is constant as confirmed by the DLS measurements.

Results and Discussion

Compound 1. The photophysical properties of the newly synthesized fluorescent silane **1** were investigated both in aerated and deoxygenated ethanol solutions. The compound shows the typical structured absorption and fluorescence bands of the pyrene chromophore (Figure 1). A comparison with the parent compound 1-methylpyrene (**2**) shows that the fluorescence quantum yield $\Phi = 5.6 \times 10^{-2}$ (6.9×10^{-2} for **2**) and fluorescence lifetime $\tau = 21$ ns (16 ns for **2**) are slightly affected by the presence of the silane-terminated chain which partially reduces the rate of the excited-state radiative deactivation. The quantum yield and excited-state lifetime of both compounds increase an order of magnitude if oxygen is excluded from the solution ($\Phi = 0.46$, $\tau = 264$ ns for **1** and $\Phi = 0.84$, $\tau = 216$ ns for **2**). The ability of oxygen molecules to quench the singlet excited state of pyrene via dynamic energy transfer processes is well documented[11] and is responsible for the relative low quantum yield of this family of fluorophores in aerated solution. The formation of the excited oxygen singlet state upon excitation of the pyrene was confirmed by the presence of the typical phosphorescence band of this species centered at 1276 nm in the NIR luminescence spectrum (Figure 2, inset).[12]

Nanoparticles N1A. Silica nanoparticles doped with 0.1% of **1** (mol/mol with respect to TEOS) show the growth profile reported in Figure 3. After a nucleation time of 15 ± 1 min the volume of the nanoparticles, measured by DLS, increases according to eq 3 with a kinetic constant (eq 3) $k = (1.4 \pm 0.1) \times 10^{-2}$ min^{-1} until a final diameter of 90 ± 10 nm. The final concentration of nanoparticles, 3×10^{-9} M, is consistent with a complete condensation of the precursors while the quantitative inclusion of the dye in the nanoparticles was confirmed by ultrafiltration experiments: only traces of unreacted pyrene could be, in fact, detected in the ultrafiltered solutions. These observations allowed us to calculate the average number of dye molecule per nanoparticle, which is as high as 10^4.

(11) Montalti, M.; Credi, C.; Prodi, L.; Gandolfi, M. T. *Handbook of Photochemistry*; CRC Press: Boca Raton, FL, 2006; p 436.
(12) Bromberg, A.; Foote, C. S. *J. Phys. Chem.* **1989**, *93*, 3968–3969.

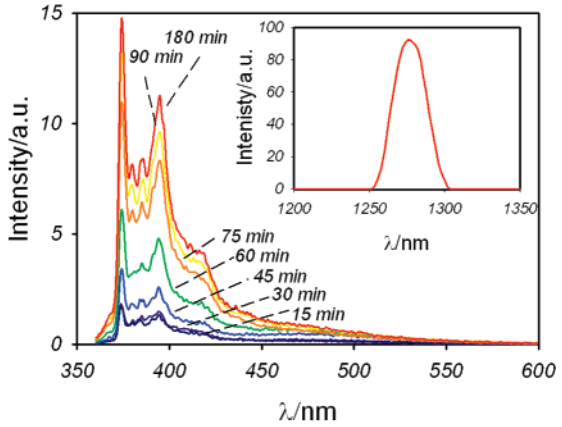

Figure 2. Changes in the fluorescence spectra upon excitation at 345 nm during the growth of nanoparticles **N1A**. Inset: luminescence spectrum in the NIR region upon excitation at 345 nm at the beginning (red line) and end (black line) of the formation of nanoparticles **N1A**.

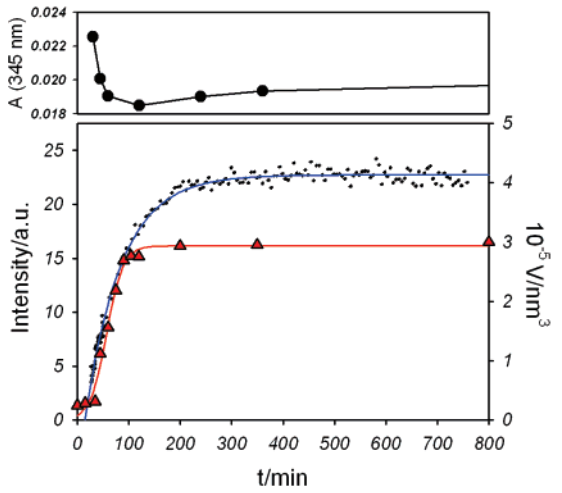

Figure 3. Fluorescence intensity at 375 nm upon excitation at 345 nm recorded during the formation of nanoparticles **N1A** (bottom, red triangles). The black dots represent the hydrodynamic volume measured by DLS (the data were fit according to eq 3). Top: absorption at 345 nm measured during the same process.

Absorption and fluorescence spectra during the synthesis were recorded by sampling small volumes of reaction mixture (0.1 mL) and diluting them to 3.0 mL with absolute ethanol in order to avoid any evolution of the system during the measurement. In addition, the dilution process also allowed us to reduce inner filter effects in the fluorescence measurement.[13] The absorption spectra recorded at different reaction times (Figure 4, inset) show that inclusion in the silica matrix causes a decrease and a gradual red shift of the structured absorption of pyrene. Fluorescence intensity, on the other hand, increases linearly with time during the first stages of the nanoparticles growth and reaches a plateau when the nanoparticles volume is 60% of the final one ($d \approx 75$ nm). Figure 3 shows that further increases of the volume of the silica structure do not correspond to any change in the fluorescence or absorbance signal of the dye, indicating that the inclusion process was already concluded (Scheme 1). The fluorescence spectrum profile on the contrary does not change during the reaction, and in particular, only a very weak contribution due to the excimeric emission could be detected

(13) Montalti, M.; Credi, C.; Prodi, L.; Gandolfi, M. T. *Handbook of Photochemistry*; CRC Press: Boca Raton, FL, 2006; pp 561−581.

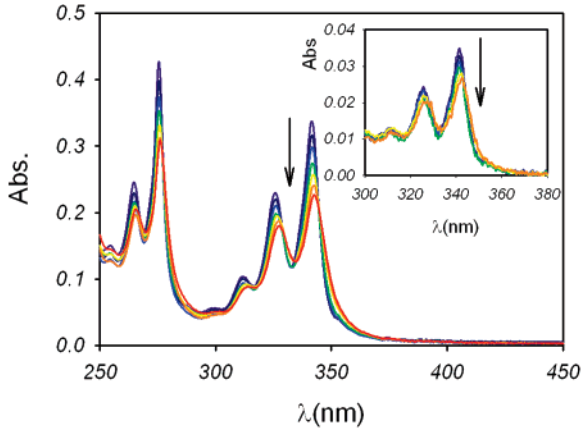

Figure 4. Changes in the absorption spectra during the growth of nanoparticles **N1B** and **N1A** (inset).

(Figure 2). The extent of the fluorescence increase confirms the quantitative inclusion of pyrene molecules evidenced by the ultafiltration experiments: the quantum yield of pyrene rises in fact to 0.48 as expected for the segregation of all the dye molecules from the atmospheric oxygen. A lifetime compatible with such situation (203 ns) is measured for the fluorescent excited state. In order to confirm the inability of the included pyrene to transfer excitation energy to oxygen molecules luminescence spectra in the NIR region were recorded. The lack of formation of the singlet excited state of oxygen upon excitation of **1** after inclusion in the nanoparticles was proved by the absence of the typical phosphorescence band observed for the same compound before nanoparticles formation (Figure 2, inset).

Nanoparticles N1B. This sample was prepared with an initial 1% concentration of **1** with respect to TEOS. As in the case of **N1A** the volume increase versus reaction time could be fit according to eq 3 (Figure 5). The nucleation time is anyway, for the more concentrated sample, considerably longer, $t_n = 45 \pm 1$ min, and the rate slower, $k = (7.4 \pm 0.1) \times 10^{-3}$ min^{-1}. On the other hand, also in this case almost complete incorporation of the dye (a fraction larger the 95%) takes place while silica nanoparticles reach a slightly larger final diameter $d = 110 \pm 10$ nm. The final nanoparticles concentration, $c = 2 \times 10^{-9}$ M, is again compatible with a complete condensation of the precursors and allows us to calculate an average number of 10^5 pyrene molecules per nanoparticle. The red shift of the pyrene structured absorption band during the reaction is in the case of **N1B** more pronounced with respect to **N1A** (Figure 4) and occurs mostly during the very first phases of the nanoparticles growth (Figure 5, top). Correspondingly, a decrease of the monomeric structured fluorescence band takes place together with a linear increase of the excimeric emission. An isoemissive point at 424 nm can be spotted in this stage (Figure 6). DLS measurements reveal that such changes are associated to the formation of silica nuclei with a hydrodynamic diameter around 60 nm (Scheme 1). All these observations are consistent with the organization of small silica cores highly doped with dye **1** where the interfluorophoric distance is so short that interactions between dye molecules at the ground state causes a change of the absorption spectra more relevant than the one produced by the simple inclusion in the silica matrix.[14] Formation of excimeric excited states on the other hand is extremely favored in these nanostructures by the mutual close proximity of the

Scheme 1. Schematic Representation of the Process of Growth of Silica Nanoparticles Doped with **1**[a]

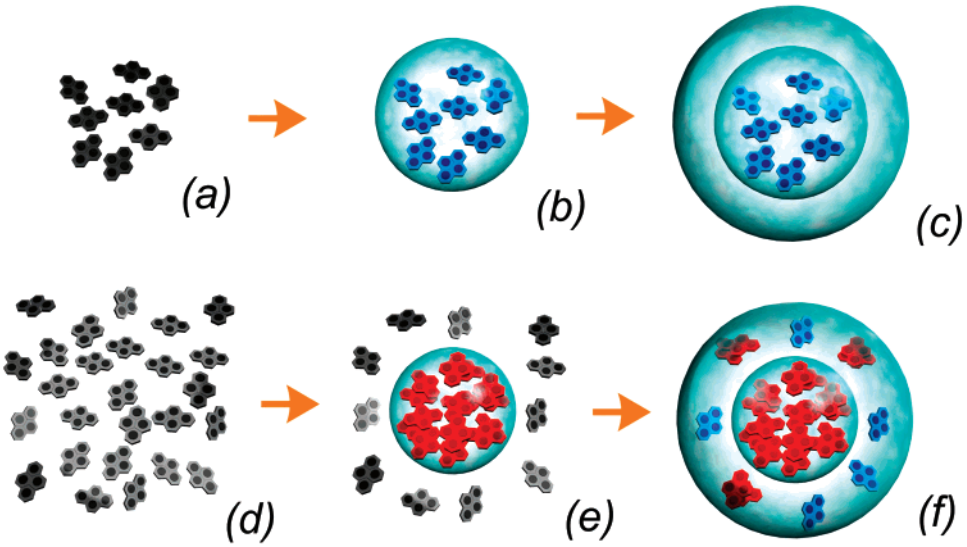

[a] Before the inclusion the dye is only weakly fluorescent because of the dynamic quenching due to atmospheric oxygen (a and d). At lower concentration (**N1A**) the dye is, in a first stage, completely included in a nucleus where its fluorescence efficiency is increased an order of magnitude; almost no excimeric emission is observed (b). A further undoped silica shell is then formed (c). At higher concentration (**N1B**) a densely doped nucleus with a characteristic excimeric emission is first produced (e). The gradual growth of a doped shell showing both monomeric and excimeric fluorescence is then observed (f).

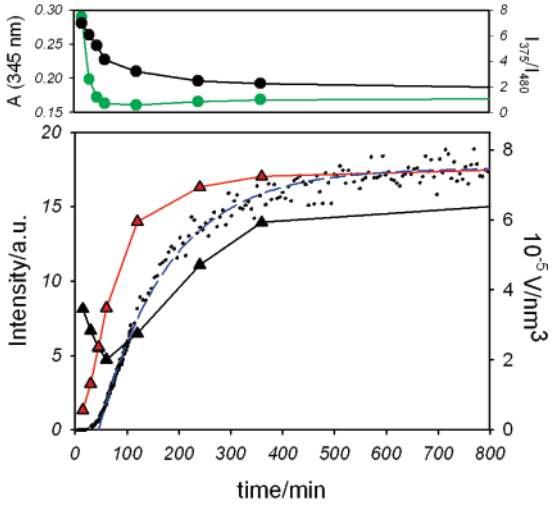

Figure 5. Bottom: fluorescence intensity at 375 (black triangles) and 480 nm (red triangles) upon excitation at 345 nm recorded during the formation of nanoparticles **N1B**. The black dots represent the hydrodynamic volume measured by DLS (the data were fit according to eq 3). Top: absorption at 345 nm (black dots) and the ratio between the two fluorescence intensity values (green dots) measured during the same process.

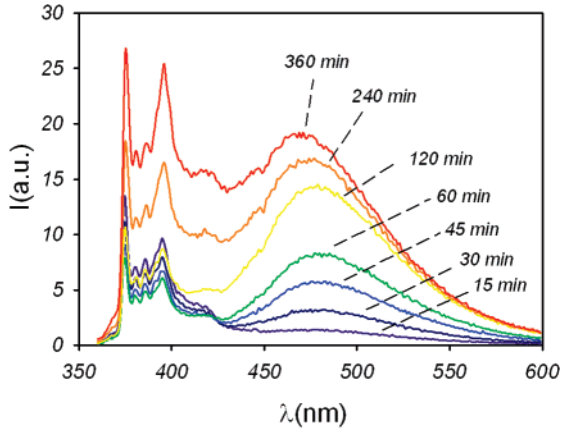

Figure 6. Changes in the fluorescence spectra upon excitation at 345 nm during the growth of nanoparticles **N1B**.

pyrene molecules, and the fluorescence spectrum of these species is dominated by a broad band centered at 480 nm. The corresponding decrease of the structured fluorescence band is related to the decrease of the concentration of the free dye responsible for such emission and can be exploited in order to evaluate the fraction of **1** included and its concentration inside the silica cores (see Scheme 1). Combination of fluorescence an DLS data indicates that about 50% of the total dye molecules are included in the silica core and show an excimeric kind of emission. The intensity ratio between the fluorescence signals at 375 and 480 nm corresponding to the maxima of the monomeric and excimeric fluorescence bands, respectively, changes slightly, after the formation of the high densely doped cores, in favor of the first kind of emission (Figure 5, top). The increase of both signals matches, in fact, in the final stage of the growth, the profile of rise of the nanoparticles volume indicating that the dye is now included at lower concentration. A gradual blue shift of the excimeric band is consistent on the other hand with a continuing increase of the average distance between the fluorophores. The TCSPC decays recorded both at 375 and 480 nm were multiexponential as expected considering the complexity of the system; nevertheless, the average excited-state lifetime for the pyrene-localized excited state was 62 ns, in agreement with the observed 3 time increase of the monomeric fluorescence at the end of the growth. An average lifetime of 65 ns for the decay of the excimeric species is in agreement with their segregation from environmental oxygen.[15]

Conclusions

Correlation of DLS and photophysical measurements gives detailed information about the inner structure of silica-doped

(14) The ground-state interactions reveal that, besides excimer, also dimer or aggregates are formed; this aspect anyway does not substantially influence the discussion.

(15) Duhamel, J.; Winnik, M. A.; Baros, F.; Andre, J. C.; Martinho, J. M. G. *J. Phys. Chem.* **1992**, *96*, 9805−9810.

nanoparticles allowing us to follow the gradual inclusion of the dye during the different stages of growth. Pyrene derivative **1** demonstrated to be a perfect dye for the investigation of the kinetics of inclusion: the fluorescent excited state of this molecule is in fact efficiently quenched by atmospheric oxygen, and a fluorescence quantum yield increase of an order of magnitude was observed because of its incorporation in the growing silica nanoparticles. The fluorescence band profile and in particular the comparison between the excimeric and monomeric contributions gave, on the other hand, information about the local concentration of the dye during the different stages of the nanoparticles growth. The compartmentalization of the fluorophore molecules in the silica matrix to give core−shell architectures could hence be revealed. We observed that if the growth of the nanoparticles takes place in the presence of low concentration of dye, all the pyrene molecules are incorporated in an inner nucleus, having a volume which is 60% of the total one, around which an undoped protecting silica shell spontaneously forms. At higher concentration, a rapid increase of the excimeric emission of the pyrene in the first stages of growth revealed the formation of small, high densely doped nuclei. A gradual increase of the monomeric emission in the following stages of the growth indicated the formation of a less densely doped shell. Besides the fraction of dye included in the nanoparticles was in both concentration regimes close to unity, larger nanoparticles were obtained in the presence of a higher concentration of the dye. The volume difference matches the different amounts of included material: 10^4 and 10^5 fluorescent molecules per nanoparticle, respectively, at low and high concentration. As far as kinetics is concerned, DLS measurements revealed during the experiments the presence of a single monodisperse population of nanoparticles with a hydrodynamic volume which rises exponentially during the time until the final value after an initial nucleation time.

Despite dishomogeneity in the photophysical behavior of fluorescent dyes that has been evidenced by some authors because of the nanoenvironment variability inside the nanoparticles, this is the first demonstration of the concentration dishomogeneity present in these nanostructure, a very important issue for the design of new materials.

Acknowledgment. This work has been supported by MIUR through FIRB 2003−2004 LATEMAR (http://www.latemar.polito.it>www.latemar.polito.it).

JA073150J